J Mar Sci Technol (2005) 10:82–95
DOI 10.1007/s00773-005-0191-4

Journal of
Marine Science
and Technology

Sail–sail and sail–hull interaction effects of hybrid-sail assisted bulk carrier

Toshifumi Fujiwara[1], Grant E. Hearn[2], Fumitoshi Kitamura[1], and Michio Ueno[1]

[1]National Maritime Research Institute (NMRI), 6-38-1 Shinkawa, Mitaka, Tokyo 181-0004, Japan
[2]School of Engineering Sciences, University of Southampton, Highfield, Southampton, UK

Abstract In a previously reported study, wind tunnel experiments were undertaken to investigate the aerodynamic characteristics of hybrid-sails in isolation. Such sails are seen as providing a worthwhile reduction in the delivered power to the propeller and hence the engine generated thrust, with a corresponding reduction in the CO_2 production of diesel engine exhaust. In this paper, wind tunnel testing is used to investigate sail–sail interaction effects for two sets of four identical hybrid-sails, and the sail–hull interaction effects for the same two sets of four identical sails in the presence of a bulk carrier hullform. The analysis presented suggests that to build a sail-assisted ship requires an appreciation of the sail–sail and sail–hull interaction effects.

Key words Global warming control · Wind tunnel experiments · Aerodynamic sail characteristics · Sail–sail and sail-hullform interaction · Sail-assisted ship

Introduction

The environmental impact of global warming is of concern to the marine industry because of the large amounts of fossil fuels used and the associated releases of CO_2 into the atmosphere. It is, therefore, very important to promote the adoption of using natural energy to reduce the required in-service delivered power of a ship. Whilst reverting completely to sailing ships may be seen as regressive, new technologies can be used to design effective sail-assisted ships. Whilst reduced CO_2 emissions can be achieved, there is a need to balance economic viability and environmental advantages. The thrust derived from sails may be viewed as applying natural energy with little negative environmental impact.

Address correspondence to: T. Fujiwara (fujiwara@nmri.go.jp)
Received: May 6, 2004 / Accepted: January 13, 2005

The idea of sail-assisted motor ships[1–4] was first addressed when fuel prices soared in an oil crisis some 20 years ago. In this case, rectangular rigid sails were formed into a circular arc and rigidly connected to the masts that were installed on the deck of a ship, see Figs. 1 and 2. The tanker form[2] in Fig. 1 has an L_{PP} of 66 m and two rectangular rigid sails with a total sail area of 194.4 m^2. The larger bulk carrier[4] in Fig. 2 has an L_{PP} of 152 m with two rectangular rigid sails of 640 m^2 total area. The effectiveness of the sail-assisted ships was confirmed in Japan[1–3] by model and full scale ship experiments. In the 1980s, about 14 sail-assisted ships were constructed in Japan. However, once the high fuel prices fell significantly, the advantages of the sail-assisted ships decreased as sail construction, maintenance, and operation were now seen as an unnecessary cost rather than a fuel cost saving device.

Currently, global warming is a political and an environmental issue, and therefore it is very important to reduce the CO_2 content of ship exhaust. New types of rigid sail have recently been examined by Rosander and Bloch[5] in Denmark. However, the construction of the Danish sail presented in Fig. 3 is very complex. The authors are of the opinion that the geometric and constructional complexity of these designs led their designers to conclude that the new rigid sails lacked financial viability. On the other hand, Nojiri et al.[6] proposed a more practical hybrid-sail that consists of a slat, a rigid wing sail and a triangular soft sail. This hybrid-sail is simpler in construction than the Danish sail and has a higher lift coefficient that the rectangular rigid sails of Ishihara et al.,[1] Matsumoto et al.[2] and Hamada.[3]

In National Maritime Research Institute (NMRI), the aerodynamic characteristics of hybrid-sails consisting of a slat, a rigid wing sail and a rectangular soft sail, see Fig. 4, have been investigated using wind tunnel experiments[7,8]. Fujiwara et al.[8] have confirmed that the rectangular soft sail based hybrid-sail is more effective than the triangular soft sail based hybrid-sail of Nojiri et

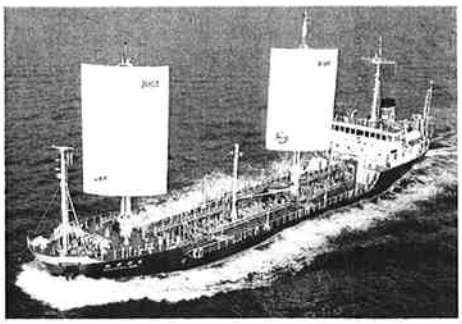

Fig. 1. Sail-assisted ship *Shin Aitoku Maru*[2]

Fig. 2. Sail-assisted ship *Usuki Pioneer*[4]

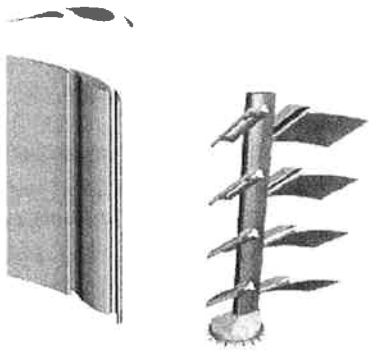

Fig. 3. Danish wing mast.[5] **a** External view of the wing mast, and **b** tacking condition of the wing mast

al. However, the triangular based hybrid-sail is easier to construct. In previous wind tunnel based experimental studies[7,8] the aerodynamic characteristics of single isolated hybrid-sails of different size and aspect ratio were investigated. Minami et al.[9,10] utilised the measured aerodynamic characteristics of an isolated hybrid-sail provided by Fujiwara et al.[7,8] to analyse the steady sailing performance of the ocean-going bulk carrier presented in Fig. 5.

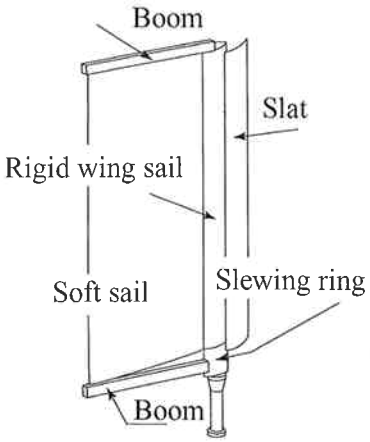

Fig. 4. Hybrid-sail consisting of a *slat*, a *rigid wing sail* and a *soft sail* attached to a *boom*

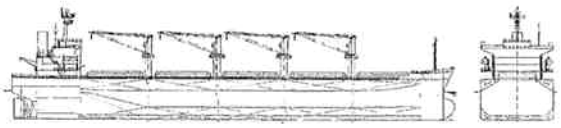

Fig. 5. Geometric form of the bulk carrier modelled

To extend the steady sailing performance analysis of a ship, more extensive aerodynamic characterisation of the sails is required to provide assessment and understanding of the effect of the sail–sail interaction and sail–hullform interaction for a practical sail configuration. Searches of literature in the public domain have not identified any research associated with sail–sail or sail–hullform interaction effects, or the assessment of such interaction data on steady sailing performance. This paper addresses the different cited interaction effects.

Experimental programme

Experimental model

The handy sized bulk carrier hullform shown in Fig. 5 is used to investigate sail–hull interaction effects. Essentially, sail-assisted propulsion can be implemented on any ship that has a large flat deck, that is, oil tankers, bulk carriers, general cargo ships etc. In fact, ships with large flat decks are a common ship form representing 70% in gross tonnes and 71% in number of the world statistics[11]. Whilst the self-discharging form of the bulk carrier presented in Fig. 5 represents a small proportion of the cited world fleet, i.e. 0.6% by gross tonnes and 0.4% in ship numbers, its selection allows this study to include the practical aspect of how to select a hybrid sail

that can be fitted to an actual ship. Having identified soft sails with preferred sizes and aspect ratio in the earlier reported studies[7,8] it would be straightforward, but less relevant, if these preferred sails were scaled down to extend our knowledge of sail–sail and sail–hull interactions. However, this would be inappropriate to the task of matching sails with the selected ship, and so the earlier information and understanding are used to provide rectangular and triangular sails that can be used with masts formed from the vertical support of each crane, subject to any clearance restrictions to be observed.

The principal particulars of the representative bulk carrier are provided in Table 1. The scale of the bulk carrier model is slightly larger than 1:150. For the representative bulk carrier hullform selected, four hybrid-sails are used with sail size and aspect ratio appropriate to the ship dimensions presented in Table 1. The dimensions and aspect ratio of the sails, see Fig. 6, are a compromise between the best rectangular and best triangular sails identified in the earlier reported study,[7,8] the crane arrangements of the selected hullform and the air draught required to allow safe operation worldwide.

Table 1. Principal ship particulars for the bulk carrier and scale model

	Ship	Model
L_{OA} (m)	185	1.254
L_{PP} (m)	177	1.200
B (m)	30.4	0.206
D (m)	16.5	0.112
d_{Full} (m)	11.6	0.079
$d_{Ballast}$ (m)	5.24	0.036
d_{Air} (m)	44.4	0.301
A_{TFull} (m^2)	553	0.025
A_{LFull} (m^2)	1997	0.092
$A_{TBallast}$ (m^2)	767	0.035
$A_{LBallast}$ (m^2)	3111	0.143

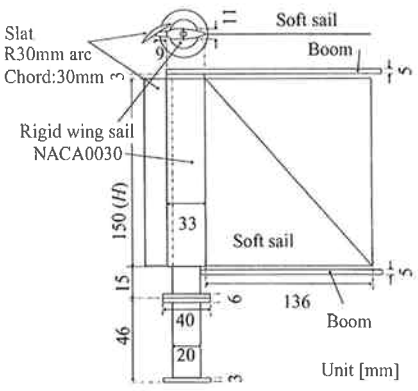

Fig. 6. Plan and side elevation of the model scale hybrid-sail

Experimental set-up

The wind tunnel experiments were carried out at NMRI. The tunnel is a closed return type, breath 3 m and height 2 m test section, and has the ability to make 30 m/s maximum wind velocity. Four distinct situations have been investigated, namely: the "single" sail in isolation, "plural" sails without hullform present, and "plural" sails in the presence of hullform with a still water plane corresponding to the ship in (a) the "full loaded" condition and (b) the trimmed "ballast" condition. For example, Fig. 7a illustrates the "plural" (four sails) arrangement for the triangular sail without hull present, whereas Fig. 7b indicates the ship in the "ballast" condition with four rectangular sails. The sails and the ship model were set up on independent turntables to facilitate changes in wind direction relative to sail or ship model (or both). The load cells to measure the longitudinal and lateral forces and the yawing moment were connected under each sail as shown in Fig. 8a. Identification of individual sails corresponds to sail No. 1 being located forward and sail No. 4 located aft. When the effect of the presence of the sails upon the loading of the ship hull was required, the load cell arrangement on the model setting changed from that shown in Fig. 8a to that illustrated in Fig. 8b.

The wind velocity was arranged to be uniform in the vertical direction apart from the thin boundary layer

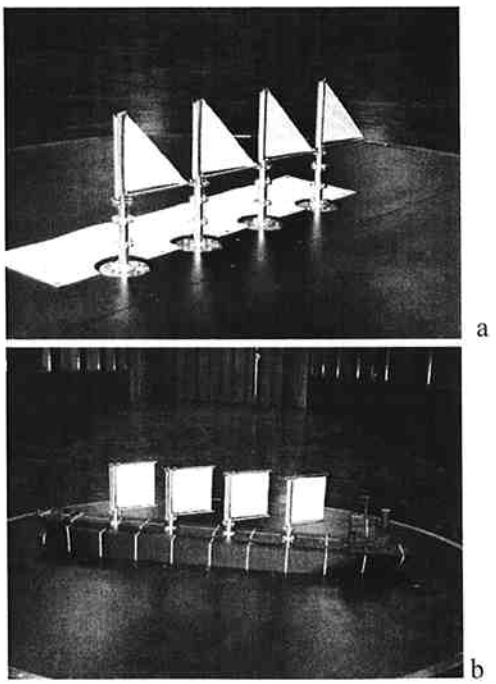

Fig. 7. **a** "Plural" experimental arrangement of the four triangular sails. **b** "Plural" arrangement of rectangular sails with the hull in the "Ballast" load condition

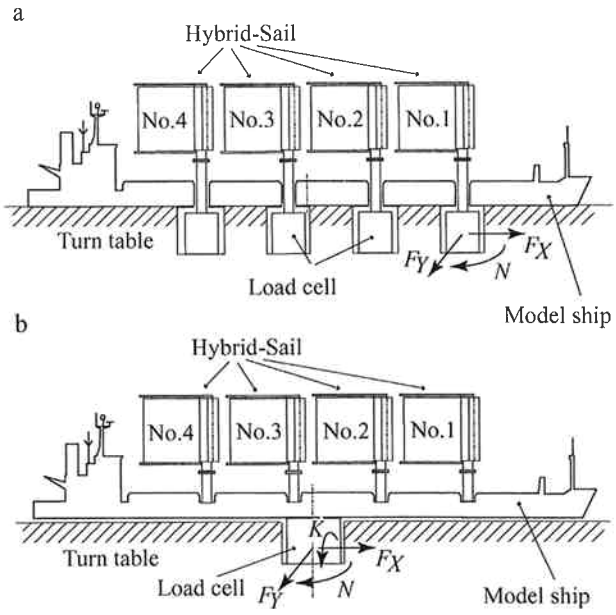

Fig. 8. Load cell arrangements for experimental measurements of sail loads and hull loads. **a** Sail loads. **b** Hull loads

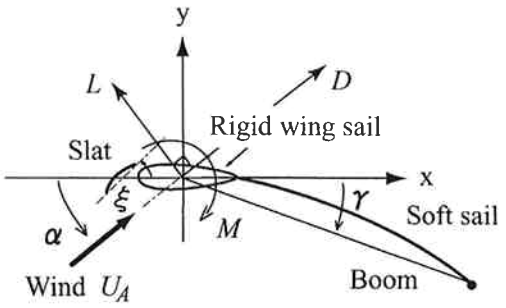

Fig. 9. Cartesian reference system and principal angles of the hybrid-sail

over the wind tunnel floor. The boundary layer has a maximum thickness of approximately 10 cm. The presence of the boundary layer is included in the specification of the average wind velocity over the model when the hullform is present. When there is no ship model present, the sails are maintained in a position and height corresponding to the hullform in its ballast condition. This is realised using supporting poles of the correct length. This arrangement is used for both the "Single" and "Plural" sail configurations in isolation. In each case the boundary layer is some distance from the lower edge of the sail, and hence the wind characterisation over the sails does not include boundary layer velocity variation.

The wind velocity selected for the investigations corresponds to a mean value of approximately 20 m/s and a Reynolds' number of 2×10^5 for a length scale based on the mean chord length of a single hybrid sail. This Reynolds' number is consistent with the earlier reported experiment.[7,8] Experimental measurements of the lift and drag coefficients with velocity variation confirmed that the selected wind velocity of 20 m/s corresponded to a turbulent flow condition, since the drag and lift coefficients were independent of Reynolds' number in this region. Hence realistic at-sea conditions were considered to prevail.

Wind force and moment coefficients

Figure 9 defines the Cartesian x–y coordinate reference system for the hybrid-sail model together with a definition of the positive lift (L) and drag (D) forces and the yawing moment (M) sign convention. The angle of attack of the apparent wind onto the rigid wing sail is designated α, whereas ξ and γ, measured with respect to the x-axis, define the orientation of the slat and boom, respectively.

With ρ_A indicating air density, U_A the apparent wind velocity, S the lateral area of a hybrid-sail, and C the mean chord length of the sail, the non-dimensional form of the lift and drag forces and the yawing moment are defined as follows:

$$C_L = L/\left(\tfrac{1}{2}\rho_A U_A^2 S\right)$$
$$C_D = D/\left(\tfrac{1}{2}\rho_A U_A^2 S\right)$$
$$C_M = M/\left(\tfrac{1}{2}\rho_A U_A^2 S C\right). \quad (1)$$

It is to be noted that S for a hybrid-sail is defined as the sum of the lateral areas of the wing sail, the slat (assumed to have a chord setting of $\xi = 35°$ with the positive x-axis) and the area of the soft sail when the boom angle (γ) is zero. This definition recognises that one must consider the actual sail arrangement in Fig. 6, because of the overlapping nature of the rigid wing sail and the slat. The mean chord C is assigned the value S/H, where H is the height of the sail (150 mm). The hybrid-sail aspect ratio (AR) is defined as H^2/S.

The hybrid-sail polar diagram relating the lift and drag load coefficients to apparent wind direction, together with the ship's course direction, is defined in Fig. 10. Assuming a zero leeway angle, the wind direction relative to ship's course is defined by ψ. The sail driving force (sail thrust contribution) and the sail side force coefficients C_X and C_Y are a function of C_L and C_D and are determined from:

$$C_X = C_L \sin\psi - C_D \cos\psi$$
$$C_Y = C_L \cos\psi + C_D \sin\psi. \quad (2)$$

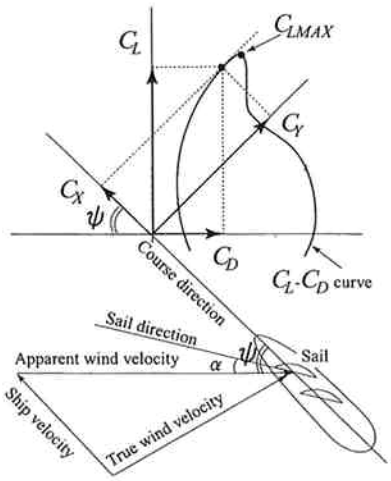

Fig. 10. Hybrid-sail polar diagram for a single sail and the associated triangle of forces for the ship

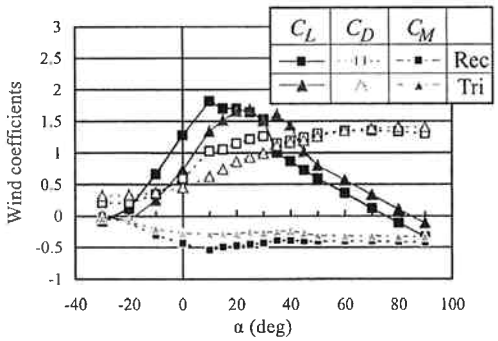

Fig. 11. Aerodynamic lift, drag and, moment coefficients for a single isolated hybrid-sail ($\xi = 35°$, $\gamma = 30°$)

Experimental results

Experimental aerodynamics characteristics and identification of single sail maximum thrust coefficient

Initially the rectangular and triangular sails are investigated in isolation. The original experimental investigations[7] indicated that the best settings of the salt and soft sail boom orientations corresponded to $\xi = 35°$ and $\gamma = 30°$. The given aspect ratio of the currently selected rectangular and triangular sails is similar to those of the previous investigations,[8] the same settings are selected in this experimental programme, i.e. AR is 0.80 for the rectangular sail (in the original study AR varied from 0.75 to 2.63.) and AR is 1.28 for the triangular sail (in the original study AR varied from 1.06 to 2.48).

Figure 11 provides the variation of the single isolated hybrid-sail values of C_L, C_D and C_M with apparent wind angle measured with respect to sail direction, as defined in Fig. 9. The maximum lift coefficient, $C_{L\mathrm{MAX}}$, is very important in terms of sail driving thrust. For the rectangular and triangular sails matched to the selected hull form one observes that the value of this coefficient is smaller than those recorded previously,[8] i.e. 1.82 and 1.68 compared to values of the order of 2.0 and 2.0 before, despite the hybrid sail models having almost the same AR values. However, because of intended sail–hull interaction investigation, the actual model sails are smaller in height in the ratio 3:10. The principal reason for the differences in the overall maximum lift coefficient has been identified as being due to the differences in the lift of the rigid wing and slat, since the lift properties of the rigid wing alone and the rigid wing and soft sail in both studies (earlier[8] and present) are comparable. Whilst the salt and rigid wing sail have comparable separation and equivalent set up conditions in terms of ξ, differences do exist in terms of the relative location and number of slat and rigid wing connections. There is also a very slight change in the structural detail of the connection piece. These small, but identified differences, which are necessary because of size differences, are responsible for the small changes in the overall lift characteristics. Were these small physical differences eliminated, it is thought that the observed coefficient differences would vanish too.

For a discrete number of wind directions, α, the lift and drag forces and moment acting on the isolated sail were measured. These values for each sail provide the polar plot in Fig. 10. Using this single sail information, one determines from Eq. 2 the value of a "virtual" ship heading ψ that would produce a maximum driving force C_X. The determined $\alpha - \psi$ relationship for each sail is as follows. For the rectangular sails α remains constant at 10° for ψ in the range 40° to 130°, whereas α remains constant at 25° for ψ in the range 135° to 160°, and α is 30° and 60° for ψ equal to 170° and 180°, respectively. For the triangular sails α changes more rapidly with ψ. In particular, α equals 10° for ψ equal to 30° and then remains constant at 20° and 35° for ψ in the ranges 40° to 115° and 120° to 160°, respectively. For ψ equal to 170° and 180°, α was found to jump to 60° and 80°, respectively.

The maximum thrust coefficient value, $C_{X\mathrm{MAX}}$, and the maximum value of the life to drag ratio $(C_L/C_D)_{\mathrm{MAX}}$ of single isolated rectangular and triangular sails are as follows:

$$C_{X\mathrm{MAX}} = 2.09, \qquad \left(\frac{C_L}{C_D}\right)_{\mathrm{MAX}} = 2.14$$

for the rectangular sail (AR = 0.80), whereas

$$C_{X\mathrm{MAX}} = 2.00, \qquad \left(\frac{C_L}{C_D}\right)_{\mathrm{MAX}} = 2.13$$

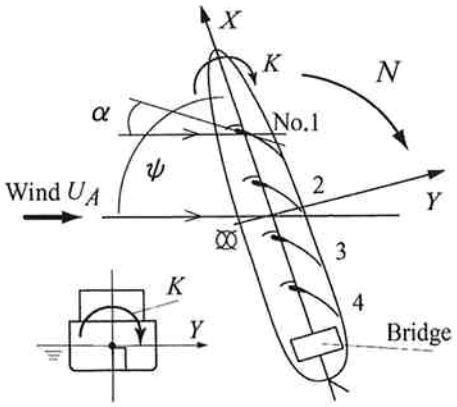

Fig. 12. Cartesian reference system of wind forces on the ship and definition of wind directions α and ψ for sail and hull

for the triangular sail (AR = 1.28). Despite the rectangular sail having a smaller AR value than that of the triangular sail, both values of $C_{X\mathrm{MAX}}$ and $(C_L/C_D)_{\mathrm{MAX}}$ are similar in magnitude.

The sail–sail and sail–hull interactions are evaluated on the basis of the single sail results in Fig. 11 using the determined $\alpha - \psi$ relationship for maximum single sail driving force in the experimental set up of Fig. 12.

Experimental results for the sail–sail and sail–hull interactions

Interactions are investigated for the four sails alone and then in the presence of a hull model in both the fully loaded and the trimmed ballasted conditions. These situations are investigated for identical rectangular sails and identical triangular sails in turn, with the same slat and fixed wing arrangement.

For each set of four identical sails the contribution to the overall driving force C_X is the force F_X measured on each sail, see Fig. 8a. In each case the vertical plane passing through the four masts is set at an angle ψ to the direction of the wind using the turntable, and the individual sails are rotated so that the wind direction relative to the symmetry axis of the rigid wing sail is equal to α, see Fig. 12. In each case this is undertaken in accordance with the $\alpha - \psi$ relationship identified for the single isolated sail maximum driving force. When the hull form is introduced, the ship position and sail orientation are set following the procedure described for the four sails investigation.

The sensitivities of maximum C_X with ψ for the case of the rectangular sail and then the triangular sail studied singly in isolation and as a set of four identical sails of fixed shape investigated with and without the presence of a hull form, under the above stated load conditions, are illustrated in Figs. 13 and 14, respectively. Individual sails within the group of four sails are identified as defined in Fig. 12. Analysis of all the data presented in Figs. 13 and 14 allows one to make the following observations:

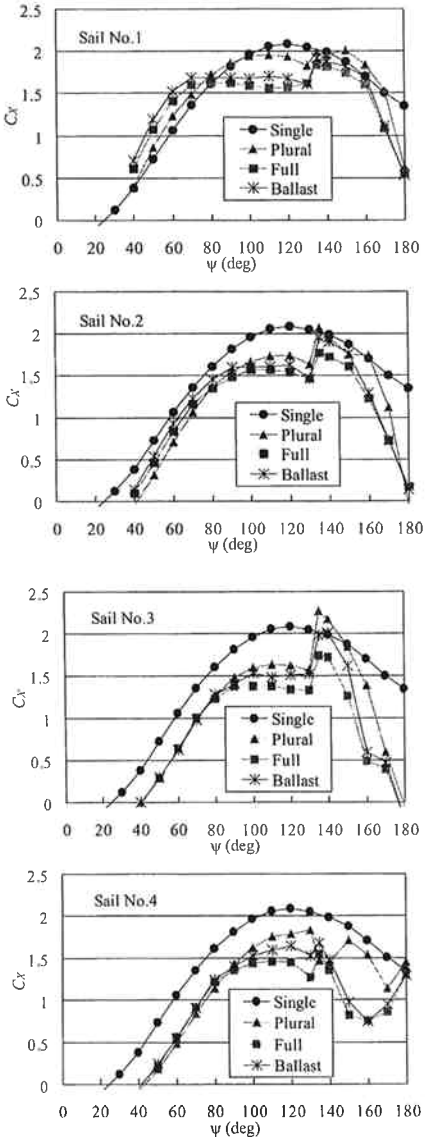

Fig. 13. Plots of individual driving-force variations of rectangular sails for each sail for each of four experimental test conditions

— Sail–sail and sail–hull interaction effects generally reduce the C_X force for each sail of either shape compared to the single isolated sail C_X values. This is particularly true when the ship is running with the wind, that is, $150° \leq \psi \leq 180°$. Physically, the cause of the sail–hull interaction in this case may be attributable to the ship bridge and sails being upwind of the sails and hence significantly affecting the airflow into the sails.
— When the ship is close hauled, that is $40° \leq \psi \leq 70°$, for sail No. 1 C_X increases (relative to the single sail

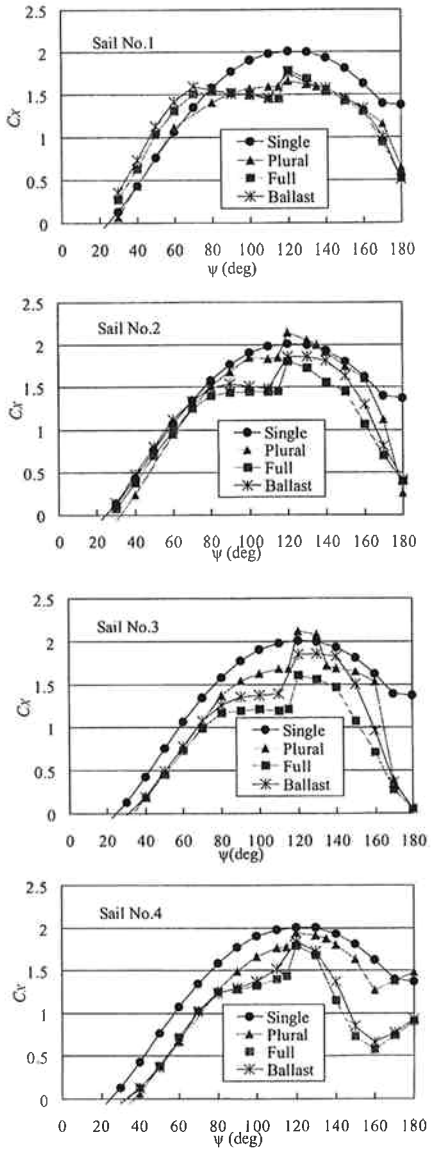

Fig. 14. Plots of individual driving-force variations of triangular sails for each sail for each of four experimental test conditions

situation) for cases of four sails with and without the hull presence, for the rectangular sail, whereas the presence of the hull rather than the other sails accounts for the C_X increase for the triangular sail.

— It is observed that C_X rapidly increases for $\psi = 135°$ on all the rectangular sails. This phenomenon occurs when $\psi = 120°$ for the triangular sails. It is possible to demonstrate that this increase is actually associated with an increase in drag rather than lift, see Figs. 26–29.

To appreciate the contributions of the sail–sail and sail–hull interaction effects, under appropriate load conditions, the average drive force differences are determined in accordance with:

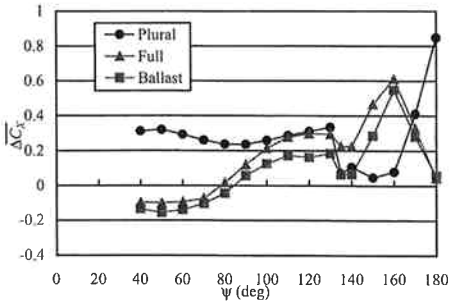

Fig. 15. Average drive force differentials for each test condition for rectangular sails

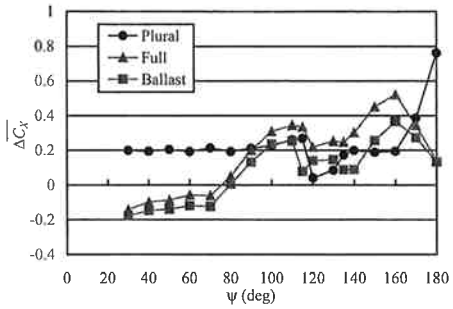

Fig. 16. Average drive force differentials for each test condition for triangular sails

$$\Delta\overline{C}_{X\text{Plural}} = C_{X\text{Single}} - \overline{C}_{X\text{Plural}}$$
$$\Delta\overline{C}_{X\text{Full}} = \overline{C}_{X\text{Plural}} - \overline{C}_{X\text{Full}}$$
$$\Delta\overline{C}_{X\text{Ballast}} = \overline{C}_{X\text{Plural}} - \overline{C}_{X\text{Ballast}}. \quad (3)$$

Here the general term $\overline{C}_{X\text{Status}}$ corresponds to averaging different components of C_X over the four sails, with status indicating the test conditions of the sails, that is, single for isolated sail, plural for the set of four sails without the hull presence, and full and ballast indicating the state of the hull presence. The different mean differences $\Delta\overline{C}_X$ for the rectangular and triangular sails are shown in Figs. 15 and 16, respectively, with positive mean difference values indicating a decreasing driving-force compared to the single isolated sail condition.

For ψ up to 60°, the mean sail–sail ($\Delta\overline{C}_{X\text{Plural}}$) and the mean sail–hull ($\Delta\overline{C}_{X\text{Full}}$ and $\Delta C_{X\text{Ballast}}$) interaction differences are of comparable magnitude but of opposite sign. For $\psi \geq 135°$ on the rectangular sails, for which α lies in the close haul range 10° to 25°, and for $\psi \geq 120°$ on the triangular sails, for which α lies in the close haul range 20° to 35°, the variance of $\Delta\overline{C}_X$ becomes large.

The assignment of α and ψ in the reported results was restricted to maximising the driving force of a single sail and maintaining a parallel arrangement with each

set of four identical sails. Next we consider the influence of two quite distinct sail arrangements upon the ship driving force.

Experimental results for sails in the graduated arrangement and in the goose-winged configuration

Wagner[12] and Bradbury[13] suggest that the "parallel" sail arrangement can be bettered. In their terms they compared parallel against graduated trim with Bradbury using a 2D potential to try and predict advantageous arrays of rigid symmetric aerofoil sails. Here the authors undertake an experimental investigation using a process they have designated the "graduated arrangement." Initially the four sails are set in the parallel arrangement (again with $\xi = 35°$ and $\gamma = 30°$) and the wind direction α increased until the resultant driving force ceases to increase. With the orientation of sail 1 unchanged, sails 2, 3 and 4 are moved in a parallel fashion, to effectively increase their angle of attack, until the total driving force again ceases to increase. Next, with sails 1 and 2 left fixed, sails 3 and 4 are moved in a parallel manner until once again no increase in total driving force is obtained, etc. Thus one derives a combination of sail settings that improve the resultant driving force, relative to the parallel setting, but this process may not have identified a global optimum setting. The increments in α, the wind setting, was 2.5° at each stage of the process described.

Figure 17a illustrates the ship model with an identified graduated arrangement of the rectangular sails. Figure 18 for the fully loaded condition and Fig. 19 for the ballast condition show how the α—values on sails 1–4 changed with the wind direction ψ for the graduated arrangement of the four sails. The results designated "para" in Figs. 18 and 19 correspond to the four sails being subject to the parallel sail setting, and in the other cases the α—values on sails 1–4 are independent of the wind directions ψ considered for the graduated arrangement of the sails. For $\psi = 60°$ and $\psi = 140°$ in the case of the rectangular sails, and $\psi = 60°$ and $\psi = 120°$ in the case of the triangular sails, the graduated arrangement provided no detectable benefit.

Averaging the four individual sail values of C_X presented in Figs. 13 and 14, and superimposing the corresponding mean values of C_X for the graduated arrangements (designated "grad") of Figs. 18 and 19 provides the comparisons in Figs. 20 and 21 for the rectangular and triangular sails, respectively. The mean values of C_X for the graduated arrangement are significantly larger than with the corresponding parallel arrangement, and in the case of the rectangular sails are more comparable with the single sail mean levels.

Another alternative sail arrangement when the ship is running with the wind is the so-called goose-winged

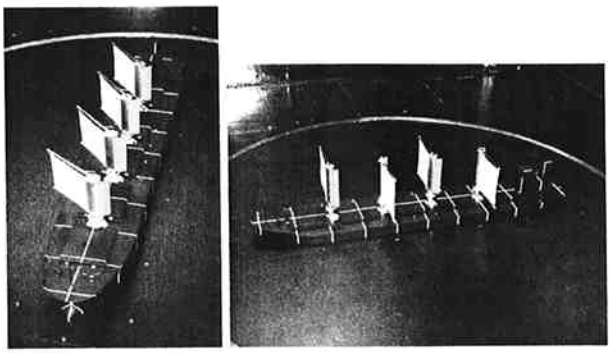

a b

Fig. 17. Photographs of the bulk carrier model with sail arrangements **a** graduated and **b** goose-winged

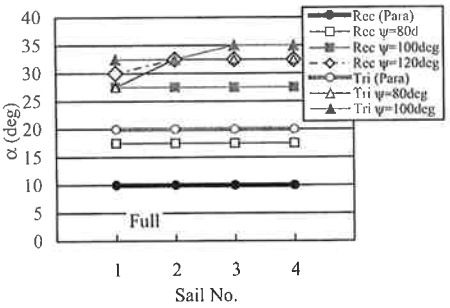

Fig. 18. Identified sail settings of rectangular and triangular sails for the graduated arrangement, for different wind directions, and for the ship in a fully loaded condition

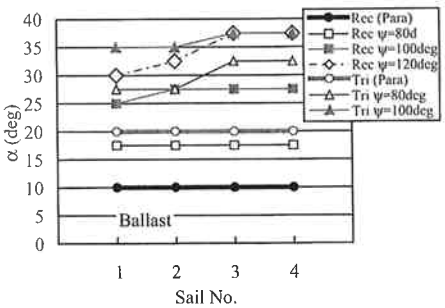

Fig. 19. Identified sail settings of rectangular and triangular sails for the graduated arrangement, for different wind directions, and for the ship in the ballasted condition

arrangement as in Fig. 17b. Here hybrid-sails 2 and 4 are to set to port and sails 1 and 3 are set to starboard with the wind corresponding to $\psi = 180°$. Figure 22 shows the mean values of C_X on sails Nos. 3 and 4 for each configuration. In the case of the goose-winged (GW) arrangement of the rectangular sails, C_X is twice the

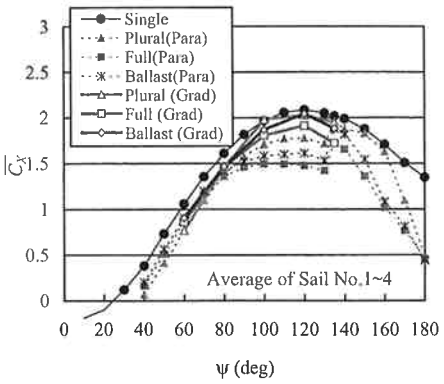

Fig. 20. Effect of the graduated sail configuration on the mean driving force coefficient for rectangular sails

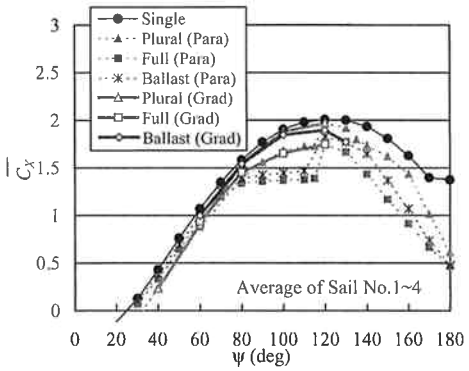

Fig. 21. Effect of the graduated sail configuration on the mean driving force coefficient for triangular sails

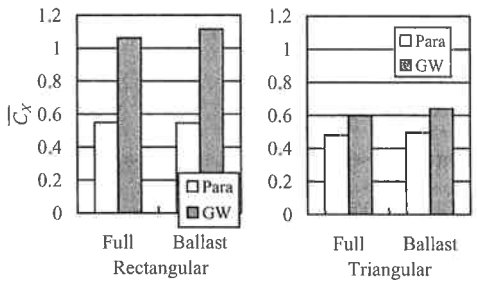

Fig. 22. Effect of the goose-winged sail configuration in the running ship condition ($\psi = 180°$) on the mean driving force coefficient of sails No. 3 and No. 4

magnitude of the parallel arrangement, but for the goose-winged triangular sails there is no apparent advantage over the parallel arrangement. This may be explained by the fact that the ship's bridge, as shown in Figs. 12 and 23, masks a large area of each triangular sail.

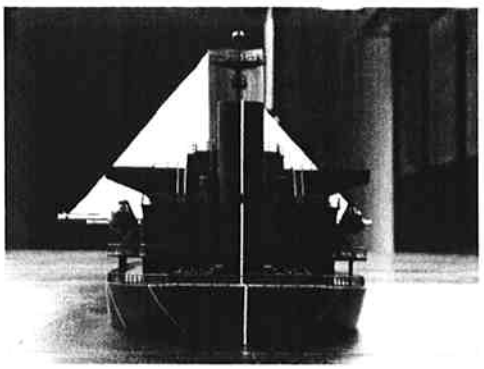

Fig. 23. Photograph of the ship stern and goose-winged triangular sails for wind in the "running" condition

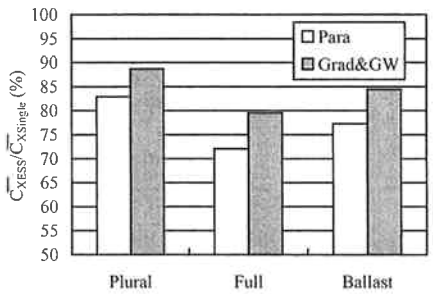

Fig. 24. Ratio of the mean driving force in different test conditions against the single isolated sail performance for different sail configurations for rectangular sails

Summary of the sail–sail and sail–hull interaction experimental results

All of the parallel measurements and the combined graduated and goose-winged measurements of the driving force coefficients $C_X(\psi)$ are now averaged with respect to the wind direction, over the wind direction range 0° to 180°, for the three cases of a set of four sails without hull presence (designated "Plural") and the set of four sails interacting with either a fully loaded ship or a ballasted ship to provide an overall mean C_X value for an "equivalent" single hybrid-sail. Figures 24 and 25 present the calculated ratio of this equivalent single sail (ESS) mean value $\bar{C}_{X\mathrm{ESS}}$ and the mean value of the single isolated sail $\bar{C}_{X\mathrm{Single}}$. From these figures one can deduce the following points:

— The difference in the ratio of the average equivalent single sail driving force and the average single sail driving force ratio (irrespective of the ship load condition) is approximately 25% for the rectangular sail system and 24% for the triangular sail arrangement.
— The graduated and goose-winged related mean levels indicate higher mean driving forces than the parallel arrangement even though the degree of

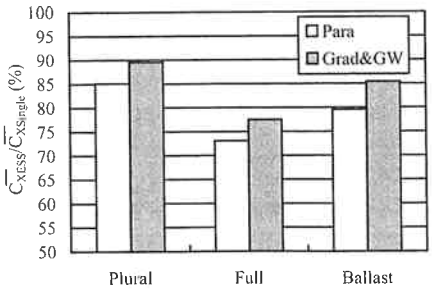

Fig. 25. Ratio of the mean driving force in different test conditions against the single isolated sail performance for different sail configurations for triangular sails

variation in α, displayed in Figs. 18 and 19, is quite small. For the triangular sail, modification of the sail arrangement does not help, whereas for the rectangular sail, the alternative sail arrangements provide a good level of recovery in the mean driving force ratio. On average, 7% of the interaction losses for the rectangular sail and 5% of the interaction losses for the triangular sail can be recovered by using a graduated or goose-winged arrangement rather than a parallel setting of the sails.

— The overall average aerodynamic performance of the deck mounted sails decreases by about 18% due to the interaction effects of the selected sails and hullform.

— Irrespective of the soft sail shape, the lowest average driving force occurs for the fully loaded condition with the parallel sail arrangement. Figures 13 and 14 also show that the contribution to the driving force from each sail is most affected by the presence of the hull form in its fully loaded condition. This observation is consistent with the occurrence of a turbulent boundary layer flow over the deck; a phenomenon was observed using smoke visualisations.

— The rectangular soft sail system is generally more efficient than the triangular soft sail system.

To investigate the general aerodynamic characteristics of the rectangular and triangular sail based hybrid sails, subject to the graduated sail arrangement, the individual sail values of C_L and C_D when the hull form is present in both the ballasted and fully loaded condition are determined. To provide an indication of how these aerodynamic conditions vary with the ship's relative wind direction, the mean values of C_L and C_D, averaged over the four sails, are reported in Figs. 26–29.

The rectangular soft sail hybrid system in the graduated sail arrangement for the hull form in a fully loaded condition (for example, see Fig. 26) indicates that both C_L and C_D increase for ψ in the range 80° to 120°. In particular, C_D increases rapidly since the sails have essentially been set at their stall angle, where the graduated arrangement increases their direction relative to the wind so that there is no further increase in lift. That is, the sail angles correspond to the settings recorded in Fig. 18. In the vicinity of the stall angle, C_L usually decreases. However, in Fig. 26 one can observe an increase in the C_L coefficient of the order of 0.2 as a consequence of the graduated arrangement. Appreciation of this last statement can be derived from consideration of a transverse row of identical sails set up in a parallel arrangement (rather than the longitudinal distribution of the reported experiments). The influence of the sails either side of the "sail of interest" induces a pressure difference on its surface consistent with the lift reduction experienced as a result of the modified circulation due to the presence of the other sails. However, in the case of a graduated arrangement, the physical separation of identical sails is narrower than that for the parallel arrangement, and consequently so is the effective angle of attack of each sail. Hence, in the selected sail arrangement it seems possible that the pressure changes induced by the neighbouring sails prevent early separation as a result of the forward sail turning the air downward over the aft sail, and this leads to a larger associated lift coefficient.

Comparing Fig. 26 with Fig. 27 and Fig. 28 with Fig. 29 shows that the trends in C_L and C_D variation are more dependent on sail shape than on the condition of the hull, especially for the graduated arrangement.

Having discussed at length the loading of the sails and their contribution to the ship driving force, completeness requires that the total effect of the wind on the sail-assisted ship be considered, as knowledge of these loads will be required in any assessment of the resulting motions of the ship.

Wind induced hull forces and moments acting on ship hull

The ship based Cartesian reference system and the force–moment positive sign convention for the wind-induced loads acting on a ship are defined in Fig. 12. The corresponding non-dimensional force and moment coefficients are defined according to:

$$\begin{aligned} C_X &= X/\left(\tfrac{1}{2}\rho_A U_A^2 A_T\right) \\ C_Y &= Y/\left(\tfrac{1}{2}\rho_A U_A^2 A_L\right) \\ C_N &= N/\left(\tfrac{1}{2}\rho_A U_A^2 A_L L_{OA}\right) \\ C_K &= K/\left(\tfrac{1}{2}\rho_A U_A^2 A_L^2/L_{OA}\right). \end{aligned} \tag{4}$$

The transverse and lateral projected areas of the ship A_T and A_L do not include the projected area of the sails, S. The resultant forces and moments acting on the ship for

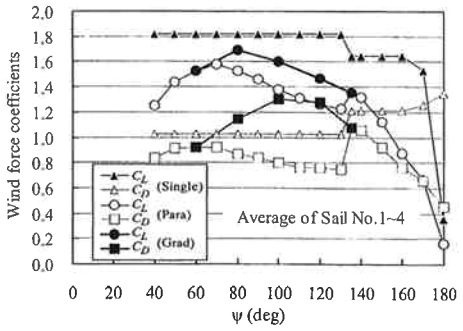

Fig. 26. Effect of the graduated arrangement of rectangular sails on C_L and C_D for the ship in the fully loaded condition

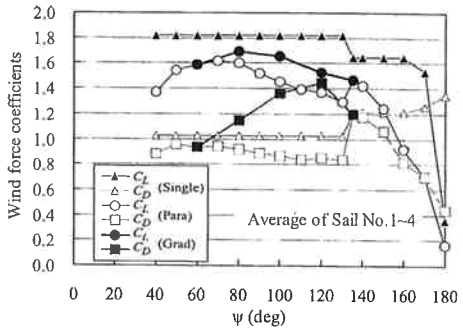

Fig. 27. Effect of the graduated arrangement of rectangular sails on C_L and C_D for the ship in the ballasted condition

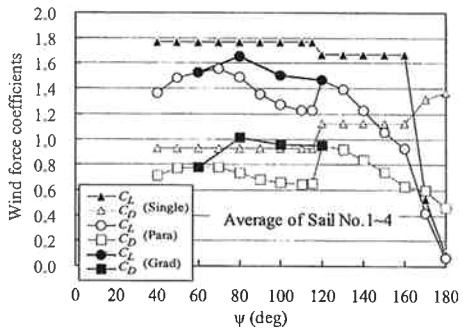

Fig. 28. Effect of the graduated arrangement of triangular sails on C_L and C_D for the ship in the fully loaded condition

the parallel, graduated and goose-winged arrangements of the sails, measured using the experimental arrangement in Fig. 8b, provide the with-interaction effect loads. The wind loads acting on the ship without the sails and the isolated sails provide estimates of wind loads without any interaction effects. When all four sails are present, interactions change as a result of the sail arrangement changing from all sails parallel to either the graduated arrangement or the goose-winged setting.

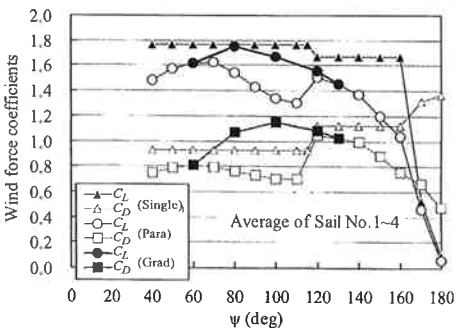

Fig. 29. Effect of the graduated arrangement of triangular sails on C_L and C_D for the ship in the ballasted condition

To appreciate the different interaction effects upon the total wind loads acting on the ship, four sets of results are presented based on measured loads under different conditions with the ship hull presented in its fully loaded and ballasted condition. Initially the wind loads on the isolated ship are considered; next the isolated ship wind loads are combined with four times the isolated single-sail wind load, corresponding to a maximum contribution to the ship driving force. These two sets of results might be expected, in general, to provide lower and upper bounds on the ship wind loads. Thereafter, the ship with the four sails set in a parallel arrangement followed by the ship with the sails set in the graduated or goose-winged arrangement are considered. In the last two cases the optimum combinations of α and ψ are to be assumed, as described in an earlier section when discussing Figs. 20 and 21. The measured wind loads under the respective umbrellas of "With int." and "Without int." are presented in Figs. 30 and 31 for the rectangular and triangular sails, respectively, for the ship in the fully loaded condition. For the ship in the ballasted condition, corresponding results are provided in Figs. 32 and 33.

Figures 30–33 clearly indicates the significant increase in the ship wind forces and moments arising from the presence of the sails. The with-interaction and without-interaction effects are mainly observed in the driving force and yawing moment, C_X and C_N. The differences in the respective total loads in Figs. 30 and 32 compared to those of Figs. 31 and 33 can be attributed to the differences in the total sail area of the rectangular and triangular sails. The driving force coefficients under ballasted conditions for both soft sail shapes, Figs. 32 and 33, are smaller than those for the fully loaded condition presented in Figs. 30 and 31. This can be explained by the fact that the transverse projected area of the ship under the ballasted condition is about one and a half times that for the fully loaded condition; see Table 1 for specific details and Eq. 4 for utilisation of detail.

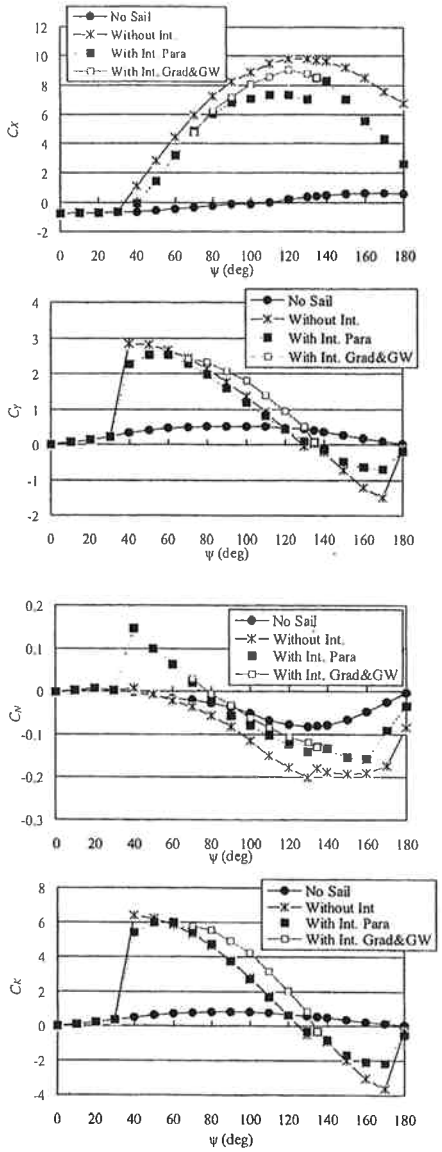

Fig. 30. Wind-dependent hull forces and moments, with and without the interaction effects of rectangular sails, for different experimental arrangements for the fully loaded ship

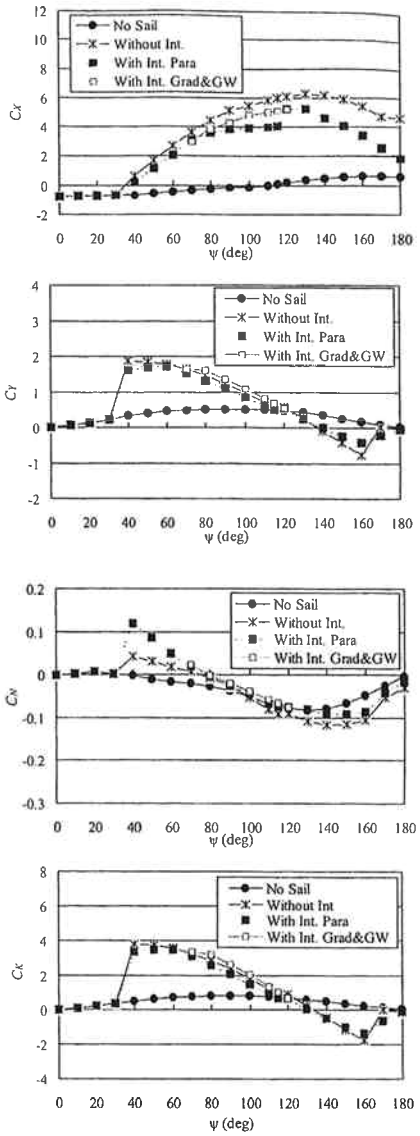

Fig. 31. Wind-dependent hull forces and moments, with and without the interaction effects of triangular sails, for different experimental arrangements for the fully loaded ship

One may also observe from Figs. 30–33 that:

— the trends, but not the magnitudes, displayed in the longitudinal and transverse loads are similar in form for both soft sail shapes, but the interaction effects are greater in the fully loaded condition;
— the interaction effects on the rolling moment coefficient are almost negligible for the triangular sails, whereas the difference due to sail arrangement (parallel versus non-parallel) are markedly different for the rectangular sails, and this has more influence than the interaction effects;
— throughout, the characteristics of the plotted transverse force coefficient and those of the rolling moment coefficient are very similar in form and dependencies;
— for the yawing moment coefficient, the interaction effects are more influential than the sail arrangement effects.

The reported experimental programme clearly demonstrates the effect of sail–hull interaction. This must be readily understood in order to estimate the navigation performance of the sail-assisted ship.

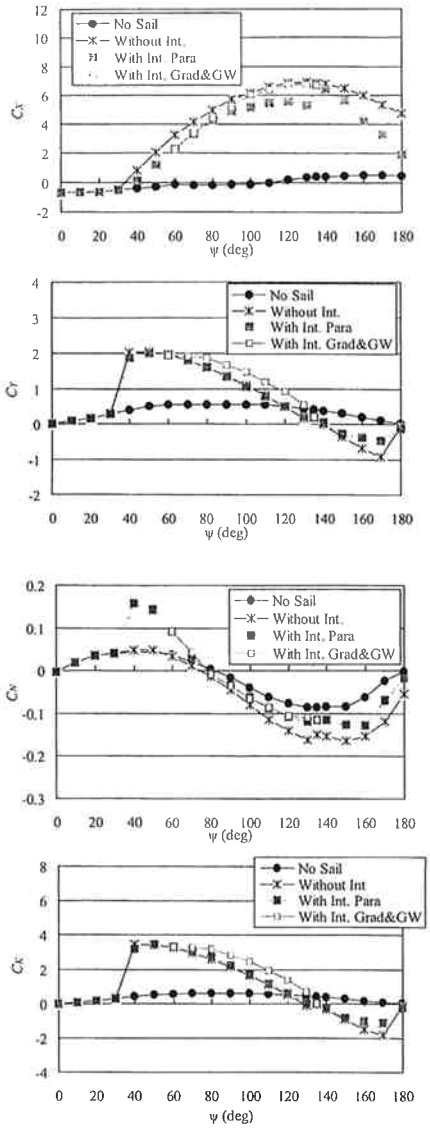

Fig. 32. Wind-dependent hull forces and moments, with and without the interaction effects of rectangular sails, for different experimental arrangements for the ballasted ship

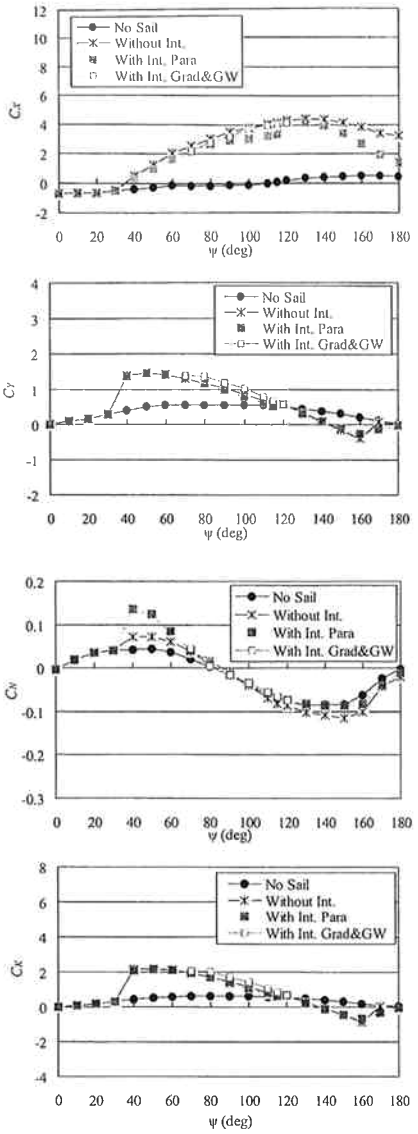

Fig. 33. Wind-dependent hull forces and moments, with and without the interaction effects of triangular sails, for different experimental arrangements for the ballasted ship

Conclusions

To reduce the CO_2 production of diesel engine exhaust relative to solving the global warming problem, the sail-assisted bulk carrier ship with hybrid-sails was examined. This new type hybrid-sail consists of a slat, a rigid wing sail and a soft sail.[7,8] The hybrid-sails investigated exhibit a significantly higher sail driving force than the 1980s rectangular rigid sail.[1–3] To extend the previous study using a single isolated sail performance, it was required to provide assessment and understanding of the more exact effect of the sail–sail interaction and sail–hullform interaction for a practical sail configuration. The results of the investigation are summarized below.

1. Sail–sail and sail–hull interactions between (i) the four rectangular and triangular type hybrid-sails and (ii) the fully loaded and ballasted conditions of a bulk carrier are clearly understood using the wind tunnel testing results. The experimental results presented suggest that to assess the quality of the sails' driving force and to build a sail-assisted ship require an appreciation of the sail–sail and sail–hull interaction effects.
2. The interaction effect is investigated using the single-sail setting for maximising the driving force. Initially

a parallel sail arrangement was maintained with each set of four identical sails for each ship's loaded condition. The difference in the average driving force for a single isolated sail and for an equivalent single sail for the present hybrid-sail when the four sails are equipped on the deck of the bulk carrier is approximately 25% for rectangular and 24% for triangular sails.

3. On average, 7% of this interaction loss for rectangular sails and 5% for triangular sails can be recovered by using a graduated arrangement or a goose-winged arrangement rather than a parallel arrangement of the sails. That is, the overall average aerodynamic performance of the sails on the deck of a ship decreases by about 18% due to the interaction effects of the sails and the hull for the selected ship form and sets of sails. However, this reduction occurs when the ship is running with wind, that is, $150° \leq \psi \leq 180°$.
4. The interaction effects between sail–sail and sail–hullform are mainly observed in the driving force coefficients and yawing moment, C_X and C_N. The interaction effects for the transverse force and rolling moment coefficients, C_Y and C_K, are very small compared to C_X and C_N.
5. The rectangular soft sail system is generally more efficient than the triangular soft sail system. This is because the interaction effect of the rectangular sails is smaller than that of the triangular sails in the case of a graduated arrangement or a goose-winged arrangement. Moreover, in the same restriction to the sails on the deck, that is, sail chord length and air draught, the rectangular sails induce more driving force than the triangular sails.

Appendix

Experimental error

Some experiments were conducted to confirm the level of experimental error. The ratio of the experimental difference Er obtained from two sets of experimental data (1st and 2nd) in the same conditions are calculated by the following equation:

$$\mathrm{Er} = \frac{\overline{C}_{X\,1\mathrm{st}} - \overline{C}_{X\,2\mathrm{nd}}}{C_{X\,\mathrm{Max}}}$$

Here, $\overline{C}_X$ is average thrust force coefficient for four sails in a wind direction measured for 10s. $\overline{C}_{X\mathrm{Max}}$ is the maximum value of $\overline{C}_X$ in the experimental series for the wind direction of $\psi = 0°$ to 180°.

In the "plural" (four sails) arrangement with rectangular type sails, Er was 0.28% for $\psi = 140°$ and 0.04% for $\psi = 170°$, obtained from experimental results carried out twice continuously. Moreover, the Er in the same arrangement, that is "plural" with rectangular sails, for $\psi = 60°$ was obtained as 1.28% after the experimental setting was changed many times. These results on Er show that the error level of the experiments is not so large and it is possible to say that the data obtained form wind tunnel experiments have enough accuracy to discuss the performance of the sail-assisted ship.

References

1. Ishihara M, Watanabe T, Shimizu K, et al (1980) Prospect of sail-equipped motor ship as assessed from experimental ship *Daioh*. Proceedings of the Shipboard Energy Conservation Symposium, Society of Naval Architects and Marine Engineers, pp 181–198
2. Matsumoto N, Inoue M, Sudo M (1982) Operating performance of a sail-equipped tanker in wave and wind. Proceedings of the 2nd International Conference of Stability of Ships and Ocean Vehicles, STAB '82, Tokyo, pp 451–464
3. Hamada N (1986) Experimental study of performance on modern sail-equipped merchant ship (in Japanese). Doctoral thesis No. 7130, Osaka University, Japan
4. Usuki Iron Works (1985) International voyage sail-equipped bulk carrier *Usuki Pioneer* (in Japanese). Funenokagaku 38:36–43
5. Rosander M, Bloch JOV (2000) Modern windships phase 2. Danish Environmental Protection Agency, http://www.mst.dk/udgiv/publications/2000/87-7944-019-3/html/default_eng.htm
6. Nojiri T, Sano K, Yagi H, et al (2003) Hybrid sail developed to show maximum lift coefficient of 2.42 for large vessels—Reduction of fuel consumption and CO_2 gas emissions expected (in Japanese). Mitsui Zosen Tech Rev 178:132–138
7. Fujiwara T, Hirata K, Ueno M, Nimura T (2003) On the aerodynamic characteristics of a hybrid-sail with a square soft sail. Proceedings of the International Society of Offshore and Polar Engineering, ISOPE2003, Hawaii, pp 326–333
8. Fujiwara T, Hirata K, Ueno M, Nimura T (2003) On the development of high-performance sails for an ocean-going sailing ship. Proceedings of the International Conference on Marine Simulation and Ship Manoeuvrability, MARSIM'03, Kanazawa, pp RC-23-1–9
9. Minami Y, Nimura T, Fujiwara T, Ueno M (2003) Investigation into underwater fin arrangement effect on steady sailing characteristics of a sail-assisted ship. Proceedings of the International Society of Offshore and Polar Eng, ISOPE2003, Hawaii, pp 318–325
10. Minami Y, Nimura T, Fujiwara T, Ueno M (2003) Comparison of underwater fin arrangement effect on performances of a sail-assisted merchant ship in North Pacific seaways. Proceedings of the International Conference on Marine Simulation and Ship Manoeuvrability, MARSIM'03. Kanazawa, pp RB-8-1–8
11. Lloyd's Register (2000) World Fleets Statistics
12. Wagner B (1967) Wind kanal versuche für einen sechsmastigen segler nach prölss. Institut für Schiffbau der Universität Hamburg, Bericht Nr. 173.1
13. Bradbury WMS (1980) An investigation of graduated trim for an aerofoil rig. Trans RI Inst Nav Archit 12:159–171